Trace Ethylene Sensing via Wacker Oxidation

ACS central science

http://pubs.acs.org/journal/acscii

Research Article

Trace Ethylene Sensing via Wacker Oxidation

Darryl Fong, Shao-Xiong Luo, Rafaela S. Andre, and Timothy M. Swager*

Cite This: ACS Cent. Sci. 2020, 6, 507−512

Read Online

ACCESS | Metrics & More | Article Recommendations | Supporting Information

ABSTRACT: Ethylene is a dynamic plant hormone, and its temporal monitoring can be used to glean insight into plant health and status. However, the real-time distributed detection of ethylene at trace levels under ambient conditions remains a challenge. We report a single-walled carbon nanotube-based chemiresistor catalyst combination that can detect ppb levels of ethylene in air. Cycling between Pd(II) and Pd(0) via Wacker oxidation with a nitrite cocatalyst imparts response discrimination driven by the chemoselectivity of the chemical transformation. Sensitivity is controlled by a combination of the chemical reaction efficiency and the n-doping strength of the Pd(0) species generated *in situ*. The covalent functionalization of the carbon nanotube sidewall with pyridyl ligands drastically improves the device sensitivity via enhanced n-doping. The utility of this ethylene sensor is demonstrated in the monitoring of senescence in red carnations and purple lisianthus flowers.

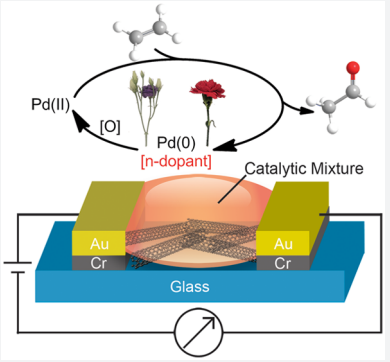

INTRODUCTION

Ethylene regulates developmental processes in flowers such as ripening, secondary metabolite synthesis, seed germination/flowering, and senescence.[1] It is recognized in biological systems by a family of five transmembrane proteins (ETR1, ETR2, ERS1, ERS2, and EIN4), each of which contributes to different ethylene response pathways.[2] Ethylene also plays a central role in stress-induced feedback loops. For example, basal ethylene production can be modulated in response to salinity, metals, hypoxia, air pollutants (O_3, SO_2, etc.), and pathogens.[3] Given the central role that ethylene plays in plant health, it is perhaps unsurprising that ethylene detection is of considerable interest to the agriculture industry. Indeed, it is estimated that upward of 50% of a farm's production value may be lost as a result of various issues along the supply chain.[4] Ethylene monitoring could reduce losses if changes in plant health are detected at an early stage and preventative actions are taken.

Ethylene detection is typically accomplished using photoacoustic spectroscopy[5] or gas chromatography.[6] Although these methods are sensitive, these analytical tools are impractical for real-time and/or in-field measurements. Other ethylene detection methods include turn-on fluorescence with luminescent polymers[7,8] or olefin metathesis catalyst/fluorescent dye hybrid molecules,[9−11] chemiresistors,[12] graphene-based field-effect transistors,[13] electrochemical oxidation,[14] and amperometry.[15] In each of these reports, there is some combination of cumbersome sensor preparation, low sensitivity, humidity intolerance, and/or sensitivity to oxygen. Given these drawbacks, there is an unmet need for the real-time robust monitoring of trace ethylene under diverse ambient conditions.

In this work, we present a highly selective ethylene chemiresistive sensor that can detect ppb levels of ethylene under ambient conditions. Our sensor is prepared from commercially available materials and leverages the sensitivity of single-walled carbon nanotubes (SWCNTs) conductance to carrier densities.[16] Specifically, we employ catalytic aerobic ethylene oxidation, wherein the palladium catalyst toggles between electron-rich Pd(0) and electron-poor Pd(II) to reversibly modulate the degree of p-doping in the SWCNTs.[17] Our method was inspired by the anti-Markovnikov Wacker oxidation initially reported by Grubbs and co-workers,[18] which uses a nitrite cocatalyst to achieve selective olefin oxidation under mild conditions (Figure 1a,b). We have demonstrated the utility of our ethylene sensor by monitoring plant senescence, which is a process that is mediated by low ppb concentrations of ethylene.

RESULTS AND DISCUSSION

Low-volatility solvents are required to avoid solvent evaporation during sensing experiments, precluding the direct translation of the reported solvent system by Grubbs and co-workers (^{t}BuOH/MeNO$_2$)[18] to chemiresistive sensing. We also substituted $AgNO_2$ with ^{n}Bu$_4$N[NO$_2$] to maintain higher solubility/uniformity. Low-volatility alcoholic solvents were screened by GC-MS using a model reaction with 1-decene and

Received: January 8, 2020
Published: March 18, 2020

https://dx.doi.org/10.1021/acscentsci.0c00022
ACS Cent. Sci. 2020, 6, 507−512

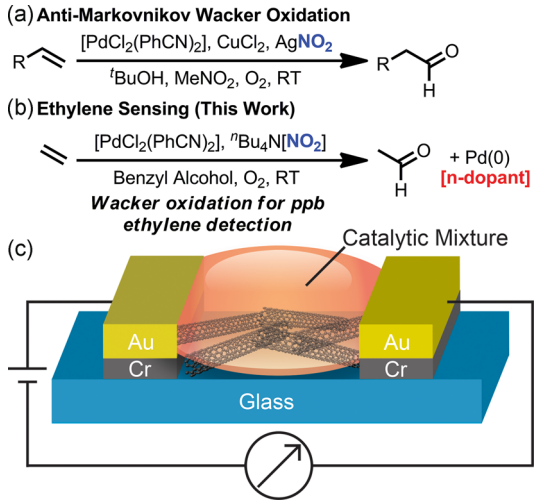

Figure 1. (a) Anti-Markovnikov Wacker oxidation with a nitrite cocatalyst reported by Grubbs and co-workers.[18] (b) Translation of catalytic aerobic Wacker oxidation for the sensitive and selective chemiresistive detection of ethylene gas. (c) Schematic of a sensing device containing gold electrodes on a glass substrate with an SWCNT network and liquid selector mixture.

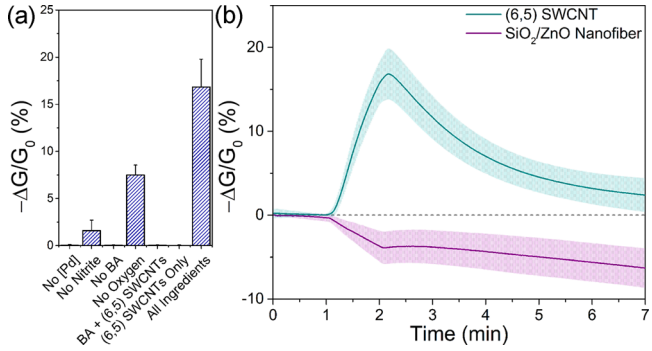

Figure 2. Exploration of the ethylene sensing mechanism. (a) Control experiments omitting $[PdCl_2(PhCN)_2]$, $^nBu_4N[NO_2]$, benzyl alcohol (BA), or oxygen. (6,5) SWCNTs only and benzyl alcohol with (6,5) SWCNTs were also tested. (b) Sensing curve using p-type (6,5) SWCNTs (green trace) and n-type SiO_2/ZnO nanofibers (purple trace) as the semiconducting material. Devices were exposed to 50 ppm of ethylene in air for 1 min ($N \geq 6$).

anisole as an internal standard (Table S1). Solvent screening revealed that benzyl alcohol, 1-decanol, and tetrahydromyrcenol afforded oxidation products of 1-decene. Removal of the alcohol moiety in the solvent had detrimental effects on total oxidation yield (<5% conversion when using toluene, benzyl cyanide, or acetophenone; Table S1, entries 6−8).

The oxidation yields were contrasted with the chemiresistive sensing response. As shown in Figure 1c, a random nanowire matrix of (6,5) single-walled carbon nanotubes (SWCNTs) is deposited between two gold electrodes on an insulating glass substrate, and then the catalytic reaction mixture is deposited on top of the SWCNTs. Device photographs and a pictorial demonstration of device fabrication are shown in Figure S1. Sensor responses are measured as the change in conductance, $\Delta G/G_0$, where ΔG is the change in conductance and G_0 is the baseline conductance in the absence of analyte. We exposed devices to 1 min of 50 ppm ethylene in air and observed no correlation between GC-MS oxidation yields and sensing responses (Figure S2). We then varied the concentrations of each ingredient using benzyl alcohol as the solvent, since it provided the strongest response from the solvent screen. Sensors having 120 mM concentrations of both $[PdCl_2(PhCN)_2]$ and $^nBu_4N[NO_2]$ afforded the largest responses to 50 ppm of ethylene (Figure S3a,b). Strikingly, removal of the $CuCl_2$ cocatalyst resulted in substantial improvement (−11.2 ± 3.6%, Figure S3c). There is literature precedence for palladium-mediated olefin oxidation in the absence of a Cu source,[19−22] and ^1H NMR studies confirm that aerobic oxidation of ethylene gas to acetaldehyde using benzyl alcohol as the solvent still occurs without $CuCl_2$ (Figures S4 and S5). We further optimized the concentration of $^nBu_4N[NO_2]$ in the absence of $CuCl_2$. As shown in Figure S6, 90 mM $^nBu_4N[NO_2]$ resulted in the strongest response of −16.8 ± 3.0%. Various commercially available conductive nanocarbon sources and palladium sources were also screened, with no response improvement (Figure S7).

We sought to corroborate our proposed sensing mechanism with some additional experiments. As shown in Figure 2a, a detrimental effect on the sensing response is observed when vital components for Wacker oxidation are omitted. The use of (6,5) SWCNTs only and benzyl alcohol with (6,5) SWCNTs exhibited a negligible response. We explored whether the generation of an n-dopant [i.e., Pd(0)] *in situ* controls the change in conductance observed. If so, then the direction of $\Delta G/G_0$ should be reversed by replacing p-type SWCNTs with an n-type material. To test this hypothesis, we prepared n-type SiO_2/ZnO nanofibers (TEM images shown in Figure S8) according to modified literature procedures.[23,24] As shown in Figure 2b, exposure to ethylene resulted in a clear increase in conductance for the n-type nanofibers, which is consistent with our proposed signal transduction mechanism. SiO_2/ZnO nanofiber-based sensors exhibited a dosimetric response and hysteresis upon repeated ethylene exposure (Figure S9). Collectively, these findings demonstrate that the *in situ* generation of Pd(0) via Wacker oxidation is responsible for a carrier reduction in the p-type SWCNTs, resulting in the observed change in conductance.

We were stimulated to further probe the role of $CuCl_2$ in the sensing response based upon the postulate of Fu and coworkers that the Pd/Cu-catalyzed anti-Markovnikov Wacker oxidation is mediated by a heterobimetallic Pd−Cu complex.[25] Considering that our sensing mechanism occurs via Pd(0) n-doping of the SWCNT sidewalls, we speculated that Pd(0) alone may be a better n-dopant than the Pd−Cu heterobimetallic complex. To test this hypothesis, we prepared devices containing pristine (6,5) SWCNTs wherein 1 μL of either the optimized Pd/Cu/nitrite or Pd/nitrite reaction mixture was deposited on top. These devices were exhaustively subjected to 1-heptene in nitrogen (to prevent reoxidation of the catalytic/dopant species) until the solvent was fully evaporated. Using Raman spectroscopy, three different spots were interrogated per sample, and the spectra were averaged. The G-band centered at ∼1590 cm^{-1} corresponds to sp^2 C−C bond stretching and shifts toward lower frequencies in the presence of electron-donating (n-doping) molecules.[26] Figure 3a summarizes the sensing response using reaction conditions with and without $CuCl_2$ present. As shown in Figure 3b, the G-band for the SWCNT sample subjected to the Pd/nitrite reaction mixture is shifted lower by 1 cm^{-1}, while SWCNTs exposed to the $CuCl_2$-containing reaction mixture are not noticeably shifted. This result is consistent with the notion that Pd(0) alone is a stronger n-dopant than the reduced Pd−Cu

https://dx.doi.org/10.1021/acscentsci.0c00022
ACS Cent. Sci. 2020, 6, 507−512

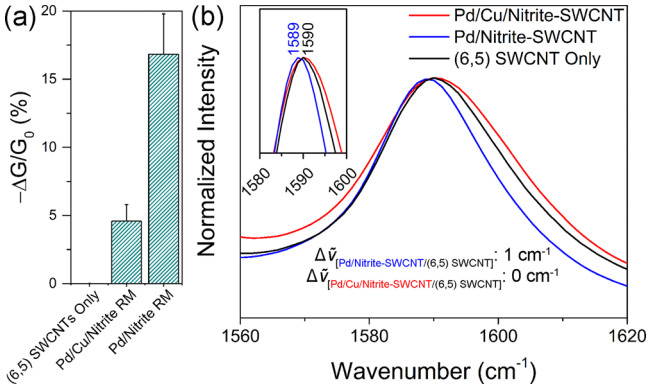

Figure 3. Investigation of the difference in sensing response when using reaction mixtures with and without $CuCl_2$. (a) Sensing responses for optimized conditions (Pd = $[PdCl_2(PhCN)_2]$, Cu = $CuCl_2$, and nitrite = $^nBu_4N[NO_2]$) and (6,5) SWCNTs only. (b) Raman spectra collected using the 532 nm excitation wavelength with spectra intensity normalized to the G-band.

heterobimetallic complex and may in part explain the observed difference in the sensing response.

We leveraged our mechanistic understanding to further improve the sensing response. We postulated that appending coordinating groups to the SWCNT surface could ensure that the Pd(0) species are localized at the SWCNT sidewall for optimal carrier modulation. We prepared 4-pyridyl-functionalized (6,5) SWCNTs using both covalent and noncovalent functionalization via iodonium salt reactions[27] and poly(4-vinylpyridine) (P4VP) polymer wrapping,[28] respectively. Covalently functionalized samples were characterized by Raman spectroscopy, X-ray photoelectron spectroscopy, and thermogravimetric analysis (Figures S10–S12). As shown in Figure 4, 4-pyridyl covalent functionalization of (6,5)

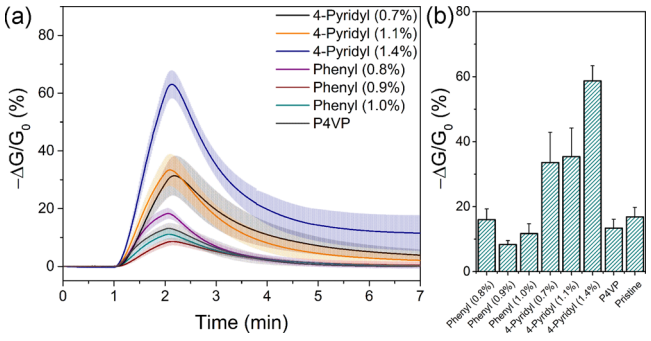

Figure 4. Sensing response using (6,5) SWCNTs functionalized covalently with 4-pyridyl or phenyl groups (0.7 −1.4 functional groups per 100 C atoms) or noncovalently with P4VP. (a) Sensing traces and (b) average device responses ($N \geq 6$). Devices were exposed to 50 ppm of ethylene in air for 1 min.

SWCNTs substantially improved the sensing response compared to pristine (6,5) nanotubes, with an increasing degree of functionalization (up to 1.4 functional groups per 100 C atoms) proving beneficial. As a control experiment, we covalently functionalized (6,5) SWCNTs with phenyl groups[27] and observed no improvement. Thus, the coordinating nitrogen atom is crucial for the observed effect. Noncovalently functionalized P4VP-coated SWCNTs did not improve device performance, which may be the result of the insulating nature of the polymer wrapping the SWCNT. As shown in Figure S13, Raman G-band analysis reveals a shift of 2 cm^{-1} upon Pd(0) doping. Although the magnitude of this shift is small, it is consistent with the notion that 4-pyridyl functionalized SWCNTs are more efficiently dedoped than pristine (6,5) SWCNTs.

Figure 5 depicts the sensitivity of our system using the optimized conditions with 4-pyridyl functionalized (6,5)

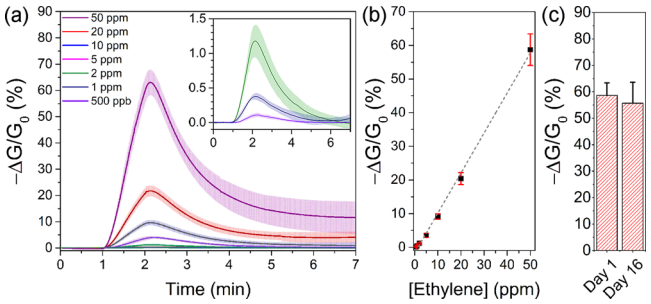

Figure 5. Sensitivity and stability of the ethylene sensor. In each condition, the reaction mixture contains 120 mM $[PdCl_2(PhCN)_2]$ and 90 mM $^nBu_4N[NO_2]$ in benzyl alcohol. (a, b) Devices were exposed to ethylene in air for 1 min ($N \geq 6$). (c) Sensor response before and after storage for 16 days at 4 °C.

SWCNTs. A clear signal is attained after a 1 min exposure to 500 ppb ethylene in air, and the responses are linear from 500 ppb to 50 ppm with a calculated limit of detection (LOD) of 15 ppb (eqs S1–S3). Using pristine (6,5) SWCNTs with other conditions the same, 500 ppb ethylene could also be detected (Figure S14). As shown in Figure S15, the devices using 4-pyridyl functionalized SWCNTs exhibited the highest response to ethylene below 40% relative humidity (R.H.), and devices delivered a consistent response when operated at 40–80% R.H. In contrast, devices using pristine (6,5) SWCNTs exhibited a continued decrease in response as the RH increased. The 4-pyridyl functionalized (6,5) SWCNTs based devices displayed limited or no degradation in sensor performance after storage at 4 °C for 16 days in the dark (Figure 5c). Some light sensitivity was observed (Figure S16a), which is a known issue for nitrite-containing liquid samples.[29] For devices using pristine (6,5) SWCNTs, some performance degradation was observed even when stored at 4 °C (Figure S16b). Overall, these results demonstrate that devices using 4-pyridyl functionalized (6,5) SWCNTs have superior sensitivity and stability compared to those using pristine (6,5) SWCNTs.

As shown in Figure 6, the selectivity of our ethylene sensor using 4-pyridyl functionalized (6,5) SWCNTs is excellent when challenged against various volatile organic compounds (VOCs). Similar selectivity was observed using pristine (6,5) SWCNTs (Figure S17a). The sensor responds to other terminal olefins and weakly to internal alkenes (Figure S17b). Even though the chemical reactivity is not expected to be markedly different between terminal olefins, the response to 1-octene was almost twice that of 1-hexene. This suggests the partition coefficient between carrier gas and liquid influences the total available olefin for oxidation.

To demonstrate the utility of our sensory system for a challenging application, we have demonstrated the ability to monitor the ethylene evolution from flowers. The flowers were enclosed in a homemade chamber, allowing us to expose the sensor to flower volatiles in a controlled manner (Figure S18). The device response to purple lisianthus flowers and red

https://dx.doi.org/10.1021/acscentsci.0c00022
ACS Cent. Sci. 2020, 6, 507−512

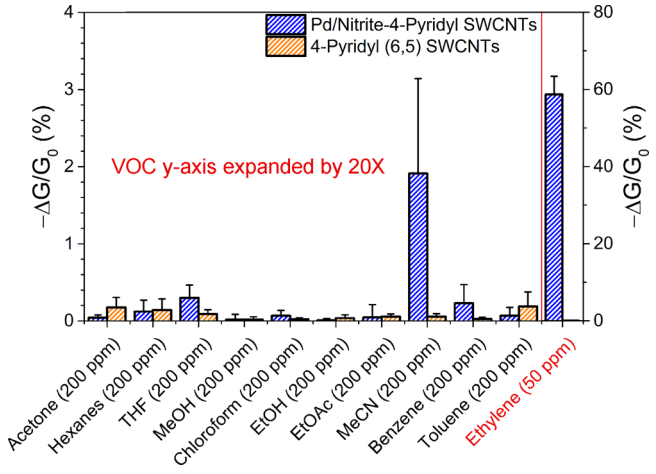

Figure 6. Selectivity in the presence of various interferents. The reaction mixture contains 120 mM Pd ($[PdCl_2(PhCN)_2]$) and 90 mM nitrite ($^nBu_4N[NO_2]$) in benzyl alcohol. Device response after exposure to VOCs in air for 1 min using 4-pyridyl functionalized SWCNTs ($N \geq 6$). The *y*-axis for VOCs is expanded by 20×.

carnations at various time points is shown in Figure 7a, and photographs of the flowers as received are shown in Figure S19. The intensities are given relative to the response to 500 ppb ethylene normalized to 100 g of flower. The flowers emitted ethylene concentrations up to ∼1.5 ppm, corresponding to an emission rate of about 320 nL·min^{-1}. Most carnation flowers bloomed within a day, while most lisianthus flowers bloomed over the period of a week. Compared to carnations, lisianthus flowers had greater variation in growth stage (Figure S20). These physical manifestations are contrasted with sensor measurements indicating rapid ethylene peaking over the span of several hours for carnations, and a gradual increase, plateau, and then decrease in ethylene evolution over the span of several days for lisianthus flowers. These ethylene profiles coincide with the observed blooming times for the flower populations and are in agreement with the known low ethylene sensitivity of lisianthus flowers[30] and high ethylene sensitivity of carnations.[31]

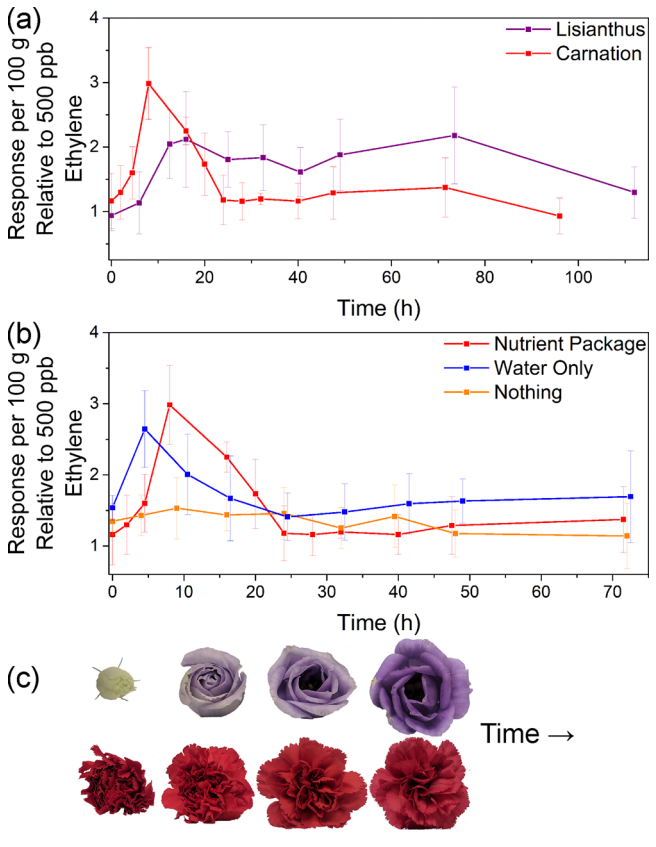

Figure 7. Flower senescence monitored using our sensory system. The reaction mixture contains 120 mM $[PdCl_2(PhCN)_2]$ and 90 mM $^nBu_4N[NO_2]$ in benzyl alcohol. Device response after exposure to flower volatiles in air for 1 min using 4-pyridyl functionalized SWCNTs ($N \geq 6$). (a) Response to purple lisianthus flowers and red carnations over several days and (b) response to red carnations treated with nothing (orange trace), water only (blue trace), or water treated with the nutrient package (red trace). (c) Photographs of lisianthus flowers and carnations over time.

Intrigued by these results, we tested whether a commercial flower nutrient package provided by the carnation supplier has an impact on the ethylene emission profile. The carnations were (i) left on the table without water, (ii) treated with water only, or (iii) treated with nutrient water. As shown in Figure 7b, when the carnations are not treated with water, no change in ethylene emission is observed. Meanwhile, treatment with water results in peak ethylene emission about 4 h earlier than treatment with nutrient water, which suggests that the nutrient packages do not strongly influence the ethylene emission profile. Gratifyingly, our sensor enables us to study dynamic plant processes mediated at low concentrations of the plant hormone ethylene.

Safety Statement. No unexpected or unusually high safety hazards were encountered in this research.

CONCLUSIONS

In summary, we have prepared a carbon nanotube-based ethylene gas sensor that uses Wacker oxidation for the selective recognition of ethylene. The devices are simple to prepare and allow us to detect ppb concentrations of ethylene in air. We demonstrate that sensitivity and stability are enhanced using 4-pyridyl functionalized carbon nanotubes. This sensory system enables us to monitor flower senescence. When translating catalytic processes into chemiresistive sensing, several lessons are revealed: (1) Reaction chemoselectivity correlates well with sensor selectivity; (2) sensitivity is controlled by both chemical reactivity and dopant efficiency, which can be tuned by the judicious selection of the catalytic components, as well as the modification of semiconductor surface chemistry; and (3) the properties of the chemical transformation (such as air tolerance) and stability of the individual reaction components translate well to sensor attributes. We foresee a continued merger of catalytic oxidation processes and chemiresistive sensing as a potent system for the facile detection of additional analytes in air and under ambient conditions.

ASSOCIATED CONTENT

Supporting Information

The Supporting Information is available free of charge at https://pubs.acs.org/doi/10.1021/acscentsci.0c00022.

Instrumentation and materials; ^1H NMR screening studies; device fabrication, optimization, and characterization; SEM of SiO_2/ZnO nanofibers; synthesis and characterization of covalently functionalized SWCNTs; additional photographs of flowers used (PDF)

https://dx.doi.org/10.1021/acscentsci.0c00022
ACS Cent. Sci. 2020, 6, 507−512

AUTHOR INFORMATION

Corresponding Author

Timothy M. Swager − *Department of Chemistry and Institute for Soldier Nanotechnologies, Massachusetts Institute of Technology, Cambridge, Massachusetts 02139, United States;* orcid.org/0000-0002-3577-0510; Email: tswager@mit.edu

Authors

Darryl Fong − *Department of Chemistry and Institute for Soldier Nanotechnologies, Massachusetts Institute of Technology, Cambridge, Massachusetts 02139, United States;* orcid.org/0000-0002-0231-683X

Shao-Xiong Luo − *Department of Chemistry and Institute for Soldier Nanotechnologies, Massachusetts Institute of Technology, Cambridge, Massachusetts 02139, United States;* orcid.org/0000-0001-5308-4576

Rafaela S. Andre − *Department of Chemistry and Institute for Soldier Nanotechnologies, Massachusetts Institute of Technology, Cambridge, Massachusetts 02139, United States; Nanotechnology National Laboratory for Agriculture (LNNA), Embrapa Instrumentação, 13560-970 São Carlos, São Paulo, Brazil*

Complete contact information is available at: https://pubs.acs.org/10.1021/acscentsci.0c00022

Notes

The authors declare the following competing financial interest(s): We plan to file a patent on this method.

ACKNOWLEDGMENTS

D.F. is grateful for support through an NSERC postdoctoral fellowship from the Government of Canada. R.D.S.A. is grateful for support through the Fundação de Amparo à Pesquisa do Estado de São Paulo (FAPESP) (Grant No. 2019/04154-9). Funding for this research was supported by National Science Foundation DMR-1809740 and U.S. Army Engineer Research and Development Center Environmental Quality Technology Program under Contract W912HZ-17-2-0027. We are grateful to Zachary P. Nelson, Samuel I. Etkind, and Dr. Máté Bezdek for insightful discussions.

REFERENCES

(1) Janssen, S.; Schmitt, K.; Blanke, M.; Bauersfeld, M. L.; Wöllenstein, J.; Lang, W. Ethylene Detection in Fruit Supply Chains. *Philos. Trans. R. Soc., A* **2014**, *372*, 20130311.

(2) Li, H.; Guo, H. Molecular Basis of the Ethylene Signaling and Response Pathway in Arabidopsis. *J. Plant Growth Regul.* **2007**, *26*, 106−117.

(3) Morgan, P. W.; Drew, M. C. Ethylene and Plant Responses to Stress. *Physiol. Plant.* **1997**, *100*, 620−630.

(4) Salunkhe, D. K.; Bhat, N. R.; Desai, B. B.; Salunkhe, D. K.; Bhat, N. R.; Desai, B. B. Senescence of Flowers and Ornamentals — Basic Principles and Considerations. In *Postharvest Biotechnology of Flowers and Ornamental Plants*; Springer, 1990; pp 13−27

(5) De Gouw, J. A.; Te Lintel Hekkert, S.; Mellqvist, J.; Warneke, C.; Atlas, E. L.; Fehsenfeld, F. C.; Fried, A.; Frost, G. J.; Harren, F. J. M.; Holloway, J. S.; et al. Airborne Measurements of Ethene from Industrial Sources Using Laser Photo-Acoustic Spectroscopy. *Environ. Sci. Technol.* **2009**, *43*, 2437−2442.

(6) Pham-Tuan, H.; Vercammen, J.; Devos, C.; Sandra, P. Automated Capillary Gas Chromatographic System to Monitor Ethylene Emitted from Biological Materials. *J. Chromatogr. A* **2000**, *868*, 249−259.

(7) Esser, B.; Swager, T. M. Detection of Ethylene Gas by Fluorescence Turn-on of a Conjugated Polymer. *Angew. Chem., Int. Ed.* **2010**, *49*, 8872−8875.

(8) Green, O.; Smith, N. A.; Ellis, A. B.; Burstyn, J. N. AgBF4-Impregnated Poly(Vinyl Phenyl Ketone): An Ethylene Sensing Film. *J. Am. Chem. Soc.* **2004**, *126*, 5952−5953.

(9) Toussaint, S. N. W.; Calkins, R. T.; Lee, S.; Michel, B. W. Olefin Metathesis-Based Fluorescent Probes for the Selective Detection of Ethylene in Live Cells. *J. Am. Chem. Soc.* **2018**, *140*, 13151−13155.

(10) Sun, M.; Yang, X.; Zhang, Y.; Wang, S.; Wong, M. W.; Ni, R.; Huang, D. Rapid and Visual Detection and Quantitation of Ethylene Released from Ripening Fruits: The New Use of Grubbs Catalyst. *J. Agric. Food Chem.* **2019**, *67*, 507−513.

(11) Vong, K.; Eda, S.; Kadota, Y.; Nasibullin, I.; Wakatake, T.; Yokoshima, S.; Shirasu, K.; Tanaka, K. An Artificial Metalloenzyme Biosensor Can Detect Ethylene Gas in Fruits and Arabidopsis Leaves. *Nat. Commun.* **2019**, *10*, 5746.

(12) Esser, B.; Schnorr, J. M.; Swager, T. M. Selective Detection of Ethylene Gas Using Carbon Nanotube-Based Devices: Utility in Determination of Fruit Ripeness. *Angew. Chem., Int. Ed.* **2012**, *51*, 5752−5756.

(13) Fu, W.; Van Dijkman, T. F.; Lima, L. M. C.; Jiang, F.; Schneider, G. F.; Bouwman, E. Ultrasensitive Ethene Detector Based on a Graphene-Copper(I) Hybrid Material. *Nano Lett.* **2017**, *17*, 7980−7988.

(14) Zevenbergen, M. A. G.; Wouters, D.; Dam, V. A. T.; Brongersma, S. H.; Crego-Calama, M. Electrochemical Sensing of Ethylene Employing a Thin Ionic-Liquid Layer. *Anal. Chem.* **2011**, *83*, 6300−6307.

(15) Jordan, L. R.; Hauser, P. C.; Dawson, G. A. Portable Trap-Sensor System for Monitoring Low Levels of Ethylene. *Analyst* **1997**, *122*, 811−814.

(16) Schroeder, V.; Savagatrup, S.; He, M.; Lin, S.; Swager, T. M. Carbon Nanotube Chemical Sensors. *Chem. Rev.* **2019**, *119*, 599−663.

(17) Schroeder, V.; Swager, T. M. Translating Catalysis to Chemiresistive Sensing. *J. Am. Chem. Soc.* **2018**, *140*, 10721−10725.

(18) Wickens, Z. K.; Morandi, B.; Grubbs, R. H. Aldehyde-Selective Wacker-Type Oxidation of Unbiased Alkenes Enabled by a Nitrite Co-Catalyst. *Angew. Chem., Int. Ed.* **2013**, *52*, 11257−11260.

(19) Ning, X. S.; Wang, M. M.; Yao, C. Z.; Chen, X. M.; Kang, Y. B. Tert-Butyl Nitrite: Organic Redox Cocatalyst for Aerobic Aldehyde-Selective Wacker-Tsuji Oxidation. *Org. Lett.* **2016**, *18*, 2700−2703.

(20) Hu, K. F.; Ning, X. S.; Qu, J. P.; Kang, Y. B. Tuning Regioselectivity of Wacker Oxidation in One Catalytic System: Small Change Makes Big Step. *J. Org. Chem.* **2018**, *83*, 11327−11332.

(21) Cornell, C. N.; Sigman, M. S. Discovery of a Practical Direct O_2-Coupled Wacker Oxidation with Pd[(−)-Sparteine]Cl_2. *Org. Lett.* **2006**, *8*, 4117.

(22) Anderson, B. J.; Keith, J. A.; Sigman, M. S. Experimental and Computational Study of a Direct O_2-Coupled Wacker Oxidation: Water Dependence in the Absence of Cu Salts. *J. Am. Chem. Soc.* **2010**, *132*, 11872.

(23) Shan, H.; Wang, X.; Shi, F.; Yan, J.; Yu, J.; Ding, B. Hierarchical Porous Structured SiO_2/SnO_2 Nanofibrous Membrane with Superb Flexibility for Molecular Filtration. *ACS Appl. Mater. Interfaces* **2017**, *9*, 18966−18976.

(24) Song, G.; Li, Z.; Li, K.; Zhang, L.; Meng, A. SiO_2/ZnO Composite Hollow Sub-Micron Fibers: Fabrication from Facile Single Capillary Electrospinning and Their Photoluminescence Properties. *Nanomaterials* **2017**, *7*, 53.

(25) Jiang, Y. Y.; Zhang, Q.; Yu, H. Z.; Fu, Y. Mechanism of Aldehyde-Selective Wacker-Type Oxidation of Unbiased Alkenes with a Nitrite Co-Catalyst. *ACS Catal.* **2015**, *5*, 1414−1423.

(26) Rao, A. M.; Eklund, P. C.; Bandow, S.; Thess, A.; Smalley, R. E. Evidence for Charge Transfer in Doped Carbon Nanotube Bundles from Raman Scattering. *Nature* **1997**, *388*, 257−259.

(27) He, M.; Swager, T. M. Covalent Functionalization of Carbon Nanomaterials with Iodonium Salts. *Chem. Mater.* **2016**, *28*, 8542−8549.
(28) Yoon, B.; Liu, S. F.; Swager, T. M. Surface-Anchored Poly(4-Vinylpyridine)-Single-Walled Carbon Nanotube-Metal Composites for Gas Detection. *Chem. Mater.* **2016**, *28*, 5916−5924.
(29) Aminot, A.; Kérouel, R. Stability and Preservation of Primary Calibration Solutions of Nutrients. *Mar. Chem.* **1996**, *52*, 173−181.
(30) Rybczyński, J. J.; Davey, M. R.; Mikuła, A. *Gentianaceae - Volume 2: Biotechnology and Applications*; Springer, 2015.
(31) Woltering, E. J.; Van Doorn, W. G. Role of Ethylene in Senescence of Petals - Morphological and Taxonomical Relationships. *J. Exp. Bot.* **1988**, *39*, 1605−1616.

https://dx.doi.org/10.1021/acscentsci.0c00022
ACS Cent. Sci. 2020, 6, 507−512